Physical simulation of trajectory tracking for tracking performance evaluation of photoelectric turntable*

WANG Guang (王光)[1,2]**, **GAO Yun-guo** (高云国)[1], and **ZHANG Shao-jun** (张绍军)[2]

1. Changchun Institute of Optics, Fine Mechanics and Physics, Chinese Academy of Sciences, Changchun 130033, China

2. University of Chinese Academy of Sciences, Beijing 100059, China

(Received 30 June 2019; Revised 23 January 2020)

Focus on the tracking target for detection indoor, the angle peak characteristics are analyzed based on uniform circular motion and the void-zone is proposed. The sine angular trajectory is used to transform the actual target into the infield, which improves the value adaptability of the peak angular acceleration to velocity and accommodates the mobility condition of photoelectric turntable. Fight trajectory is generated by a tri-axial optical target and the tracking experiment is carried out by theodolite to realize the physical simulation of trajectory, which provides powerful conditions for evaluating the tracking performance of photoelectric turntable under the mobility index.

Document code: A **Article ID:** 1673-1905(2020)04-0272-7

DOI https://doi.org/10.1007/s11801-020-9163-5

In order to complete the internal tracking detection of the photoelectric turntable, testing equipment is required to simulate the target trajectory movement with the same characteristics as actual aerial targets. The testing equipment provides the real-time motion parameters of the target as the calibration benchmark for the tracking of the photoelectric turntable[1-3]. The hardware-in-the- loop simulation of aircraft trajectory has been widely studied at home and abroad[4-6]. The visual simulation can provide the remote simulation target and its real-time motion state for the photoelectric tracking system[7-10], but it relies on computer information technology and still aims at virtual targets. Physical simulation for tracking detection indoor apply extensively the conventional dynamic target[11]. However, the simulated objective can only perform constant circumferential motion on a tilted plane, the trajectory is fixed in form, the angle range is limited in tracking, and the peak angular velocity and acceleration are interrelated meanwhile. Therefore, the simulated target moving is not representative and the tracking accuracy measured cannot evaluate truly the actual tracking performance of the photoelectric turntable. Other physical simulation equipments with different trajectory forms have been developed[12,13], which improve the traditional testing equipment.

Trajectory tracking requires the target motion to be planned and controlled[14-17], as the typical trajectories, CV, CT, CA have an important research significance[2,3]. In the process of tracking and detecting photoelectric turntable, because the optical axis is always aligned to the target, the angular velocity and acceleration of the turntable are obtained by the transformation of the moving target. Therefore, according to the different requirements of the motion maneuverability index of the turntable, it is necessary to design the target motion law reasonably.

In this study, starting with the typical circumferential trajectory and a novel tri-axial optical target (TAT) as the physical simulation equipment of the objective, target maneuvering characteristics are studied when the angular velocity and angular acceleration reach to the indexes of the turntable. The flight trajectory is designed and the physical simulation of internal trajectory is performed, which improves the value adaptability of the peak angular acceleration of tracking target to the peak angular velocity and provides an universal detection conditions for the tracking performance of optoelectronic turntable with different motion maneuverability indexes.

As the executive mechanism for simulation, the TAT is used to form the internal physical simulation trajectory, which has the advantage of outputting different trajectory motion according to actual needs. Fig.1 shows the construction of the TAT that is composed of two parts: the motion simulator and the target generator[13]. The motion simulator engenders the trajectory movement of the simulated target through the coordinated control of three axes including the rotation axis system, the aiming axis system and the linear motion axis system, and the target generator provides the simulated target light source[18] as shown in Fig.2.

* This work has been supported by the Innovation Project Funding of Changchun Institute of Optics, Fine Mechanics and Physics, Chinese Academy of Science (No.061X20C060).

** E-mail: wg_hit@163.com

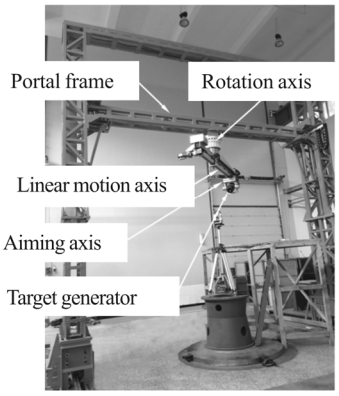

Fig.1 Construction of the TAT

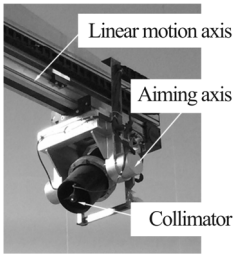

Fig.2 Target generator

The TAT control and drive the torque motors of the three-axis linkage system (LS) respectively by inputting commands. The rotation axis system of LS turns around the vertical axis, the linear motion axis system moves to make the emergent light of the target generator align to the optical axis. In the spherical coordinate system with the photoelectric turntable as the observation origin, the target generator can form a specific simulation trajectory in the horizontal plane perpendicular to the rotation axis line by controlling the movement of the three axes with a certain rule. Because of the light source being deemed at infinity and not limited by the distance, the simulated objective by the target generator can replace any space flying target, and then the changes of the azimuth and pitching of the actual target in three-dimensional space can be studied.

Taking the horizontal uniform circumferential motion as a representative movement, this paper firstly analyzes the peak characteristics of the angular motion of the aerial maneuver target in the spherical coordinate system, and deduces the peak angular motion formulas at different observation positions.

The position of the photoelectric turntable is regarded as the observation origin O. Suppose that an aerial target $P(x, y, z)$ moves at the plane of altitude h, ω is the angular frequency of circular motion, r is the radius. The center O_1 of the circle is always in the first quadrant of the plane Oyz and b is the eccentricity from O_1 to z-axis, then the shortcut flight course $l_0=b-r$. In the spherical coordinate system space $Oxyz$, the circumferential trajectory observed at a certain height plane is divided into two cases. One is the distant target which trajectory is located outside the z-axis and the azimuth angle swing back and forth, $l_0>0$, the other is the top target which trajectory moves around the z-axis and the azimuth angle rotate, $l_0<0$. Two different situations are shown as Fig.3. Take Fig.3(a) as an example, the trajectory equation of the azimuth and pitching angle are listed as

$$A = \arccos\frac{r\sin\omega t}{l}, \tag{1}$$

$$E = \arctan\frac{h}{\sqrt{l^2+h^2}}, \tag{2}$$

where $l=\sqrt{r^2+b^2-2br\cos\omega t}$ is the horizontal distance from target P to point O, and l varies from l_0 to $2b-l_0$.

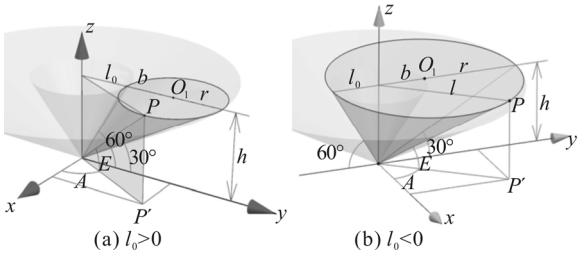

Fig.3 Horizontal uniform circular motion trail

Azimuth and pitch motion are the two motion components of the target in the spherical coordinate system, and the corresponding angular velocity and angular acceleration are not uniformly changed with the sine law, which are complex functions on time t[11,12]. Deriving Eqs.(1) and (2) once and twice respectively, the velocity and acceleration functions of the azimuth and pitching angle are given. Suppose that the position parameters $k_b=b/r$ and $k_h=h/r$, simplifying the equations and eliminating the time variable t, the formulas of each function at the corresponding peak point are obtained as

$$\dot{A}_{\max} = \frac{\omega}{1-k_b}, \tag{3}$$

$$\ddot{A}_{\max} = \omega^2\frac{k_b(1-k_b)\sqrt{1-c_A^2}}{\left(1+k_b^2-2k_bc_A\right)^2}, \tag{4}$$

$$\dot{E}_{\max} = \frac{\omega k_b k_h\sqrt{1-c_E^2}}{\sqrt{1+k_b^2-2k_bc_E}\cdot\left(1+k_b^2+k_h^2-2k_bc_E\right)}, \tag{5}$$

$$\ddot{E}_{\max} = \frac{\omega^2 k_b k_h}{\left[(1-k_b)^2+k_h^2\right](1-k_b)}, \tag{6}$$

where c_A and c_E are the functions on k_b and k_h, which can be determined by the following expressions:

$$c_A = \frac{\sqrt{\left(k_b^2+1\right)^2+32k_b^2}-\left(k_b^2+1\right)}{4k_b}, \tag{7}$$

$$2c_E^3+\frac{k_h^2+k_b^2+1}{k_b}c_E^3-\left[\left(k_h^2+1\right)\left(k_b^2+\frac{1}{k_b^2}\right)+8\right]c_E+\frac{k_h^2+3k_b^2+3}{k_b}=0. \tag{8}$$

The angular velocity and the angular acceleration of the horizontal uniform circular motion trajectory in the spherical coordinate system are calculated and analyzed by MATLAB. Suppose the radius r=1 km, the altitude h=1.73 km, the pitching angle changes from 30° to 60°, then the shortcut flight course l_0 changes at [1, +∞) and [−1, −0.5]. When selecting ω=0.53 rad/s, according to Eq.(3) to (6), the relationships between the peak angular velocity curves and the peak angular acceleration curves of azimuth are analyzed by MATLAB and shown in Fig.4. The peak angular acceleration increase with l_0 increases when the peak angular velocity is fixed, which is smallest at l_0=1 when l_0 changes at [1, +∞), and is largest at l_0=−0.5 when l_0 changes at [−1, −0.5]. So the two curves at l_0=1 and l_0=−0.5 are called the boundary curves, represented by L_1 and L_2 respectively. Under the horizontal uniform circumferential motion, the correspondence obtained between the peak angular velocity and the peak angular acceleration is in the upper left and lower right of Fig.4, and the intermediate region sandwiched by L_1 and L_2 is called the void zone of the angular movement of the uniform circumferential trajectory (V-Zone).

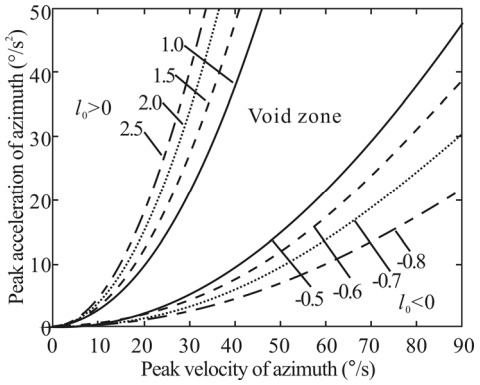

Fig.4 Angular motion maneuvering range

As said above, the observed position of the target with the angular frequency ω in the spherical coordinate space is the case that the azimuth reciprocating swing (l_0>0) or that the azimuth rotate (l_0>0). In the former case, the trajectory which is outside the z-axis can provide a larger angular acceleration[19] when the peak angular velocity is ensured. In the latter case, the trajectory which is passed by z-axis provides a smaller angular acceleration and the angular mobility slows down. Compared with the traditional target trajectory tracking[11,20], the peak characteristics of the target azimuth motion can be analyzed comprehensively. The facts are illustrated that, when the peak angular velocity is constant, the peak angular acceleration can only be changed in a limited range as the space position changes. The V-Zone exists in the circular motion because the peak angular acceleration $\ddot{A}_{\max}$ is less adaptive to the peak angular velocity $\dot{A}_{\max}$.

To get more general correspondence between $\dot{A}_{\max}$ and $\ddot{A}_{\max}$ filling the V-Zone, it is necessary to plan reasonably the different target track and improve the maneuvering range of the simulation target.

The circular motion of the target is improved for the trajectory in which l_0>0 in Fig.3(b) below. The sine angular trajectory is proposed which increases the maneuvering range and fills the V-Zone of the angle motion to meet the mobility requirements for turntable testing.

Based on the angular motion with the sinusoidal law, the periodic trajectory of the target on the height h level is designed. Combined with the correlation between the linear motion axis and the aiming axis of the TAT, the equation of the sine angular trajectory is given:

$$\begin{cases} A_e = \omega_{Ae0}\left(t - \dfrac{2k\pi}{\omega_{Ae0}}\right) - A_{me}\sin\left(\omega_{Ae1}t\right) \\ E_e = E_0 - E_{me}\cos\left(\omega_{Ee}t\right) \\ l = \dfrac{h}{\tan\left(E_e\right)} \end{cases},$$

$$t \in \left[2k\pi, 2\left(k+1\right)\pi\right], k = 0,1,2.....\,, \tag{9}$$

where ω_{Ae0} is the rotation angular frequency, A_{me} is the vibration amplitude, and ω_{Ae1} is the vibration angular frequency of the azimuth. E_0 is the center position of swing, E_{me} is the amplitude, and ω_{Ee} is the angular frequency of the pitching. h and l represent the flying altitude of the target and the horizontal distance from the observation point respectively. Different from the original horizontal circular trajectory in Fig.3, the azimuth and pitching angle obey the angle sine rule, and the trajectory curve formed by the above equation is an approximately circular path.

To ensure the azimuth's periodicity of 360° under the condition of velocity fluctuation, and the target tracking's periodicity formed by the linkage of azimuth and pitching, it is necessary to have the following multiple relation formula on angular frequency:

$$\omega_{Ae1}=n_1\omega_{Ae0},\ n_1=1,\ 2,\ \ldots, \tag{10}$$

$$\omega_{Ee}=n_2\omega_{Ae0},\ n_2=1,\ 2,\ \ldots, \tag{11}$$

where n_1 and n_2 represent vibrations of the corresponding azimuth and pitching angles per rotation period.

According to the equivalent sine method[21]. A_{me} and ω_{Ae1} above can be obtained by $\dot{A}_{\max}$ and $\ddot{A}_{\max}$. Let k=0 in Eq.(9), the azimuth within a period from 0° to 360° is analyzed. Differentiate A_e above and bring Eq.(10) into the derived function, then the relation between $\ddot{A}_{\max}$ and $\dot{A}_{\max}$ is given:

$$\ddot{A}_{\max} = \frac{n_1^2 A_{me}}{\left(n_1 A_{me}+1\right)^2}\dot{A}_{\max}^2, \tag{12}$$

$$\ddot{A}_{\max} = n_1\omega_{Ae0}\left(\dot{A}_{\max} - \omega_{Ae0}\right). \tag{13}$$

Choosing the appropriate n_1, then A_{me} and ω_{Ae1} can be determined. The following inequality is easily got from Eq.(12):

$$\ddot{A}_{\max} \le \frac{n_1}{4}\dot{A}_{\max}^2 . \quad (14)$$

If and only if n_1A_{me}=1, then the equal sign is valid. This relation curve this moment is called the boundary curve L_e. As shown in Fig.5, the larger n_1, the faster $\ddot{A}_{\max}$ goes up with $\dot{A}_{\max}$. The peak angular acceleration $\ddot{A}_{\max}$ can be reached in the lower right region of the curve L_e in Fig.5 when selecting different n_1 and A_{me}.

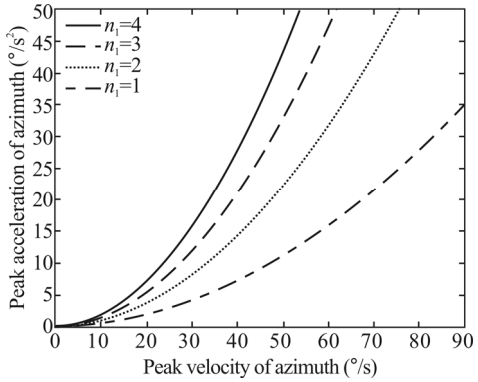

Fig.5 The relationship curve between peak angular velocity and peak angular acceleration at different n_0

In contrast to Fig.4, the boundary curve L_e changes gradually from the position of L_2 to L_1 as n_1 increases, that is, the V-Zone is swept by L_e until it is filled fully. It can be said that the sine angular trajectory increases the applicable range of the angle motion carrying uniform circumferential trajectory previously, the value adaptability of the peak angular acceleration relative to the peak angular velocity is enhanced, the sine angular trajectory of the simulated target can be used to complete the universal detection for tracking performance of the photoelectric turntable with different moving maneuverability indexes by complementing the horizontal uniform circular trajectory.

Based on the equivalent sine method[21], the sine angular trajectory above add the parameter n_1 by the rotation angle frequency ω_{Ae0}, which make the target maneuver cannot only meet the requirements of the maximum angular velocity and the maximum angular acceleration index of the theodolite motion, but also complete the whole cycle motion on the azimuth angle. Meanwhile, compared to traditional tracking targets[11,20], TAT can independently control the azimuth and pitch axis motion[22], and the angular motion has the ideal sine law. The sine angular trajectory combines the traditional target with the equivalent sine theory, which simplifies the operation, realizes the control method easier and provides a more adaptable simulation target for photoelectric turntable detection.

Utilizing the TAT to generate the sine angular trajectory of the simulated target, the tracking experiment is carried out practically by the photoelectric turntable to realize the internal physical simulation of the trajectory tracking. A type of theodolite is selected for target tracking in the experiment which has the tracking accuracy of 1.375' (0.4 mrad). The maximum working angular velocity and acceleration are 30°/s and 15°/s^2, respectively.

The tracking experiment is shown in Fig.6. The peak angular acceleration of the simulated target motion varies from 0°/s^2 to 15.7°/s^2 while the peak angular velocity is 30°/s when selecting n_1=4 from Eq.(14) and Fig.5, and the maximum angular velocity and acceleration can be obtained by the theodolite at this time. The theodolite's tracking performance is required to be measured in its maximum maneuverable state. To round the period of the azimuth motion, $\dot{A}_{\max}$=30°/s and $\ddot{A}_{\max}$=14°/s^2 are chosen. Supposed that the pitching E ranges from 41° to 49°, and n_2=1 is selected. The above values are led into Eqs.(12) and (13), then the parameters in Eq.(9) are obtained in Tab.1.

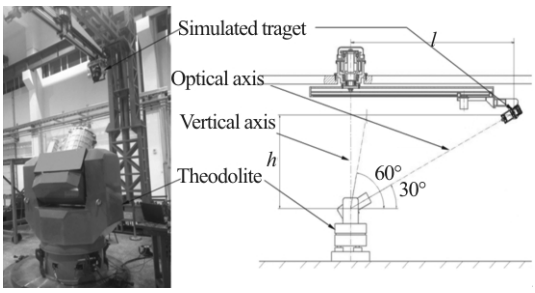

Fig.6 Tracking experiment of theodolite

Tab.1 The values for parameters of the sine angular trajectory equation

A_{me} (°)	ω_{Ae0} (rad/s)	ω_{Ae1} (rad/s)	E_0 (°)	E_{me} (°)	ω_{Ee} (rad/s)
7.2	0.35	1.4	45	4	0.35

The TAT generates the trajectory of the simulated target according to these parameters. The angular and track data of the azimuth and pitching motion are obtained through tracking and detecting by theodolite, which is used to draw the corresponding curves and fit the angular velocity and acceleration curves with sinusoidal function in Figs.7 and 8.

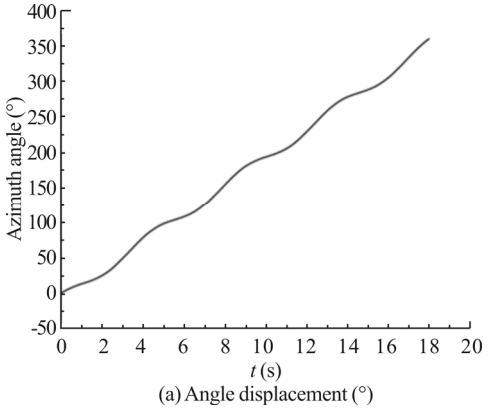

(a) Angle displacement (°)

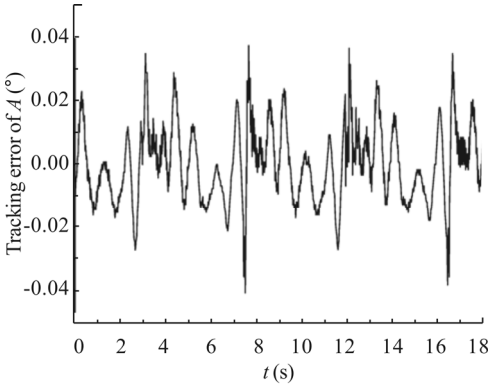

(b) Tracking error (°)

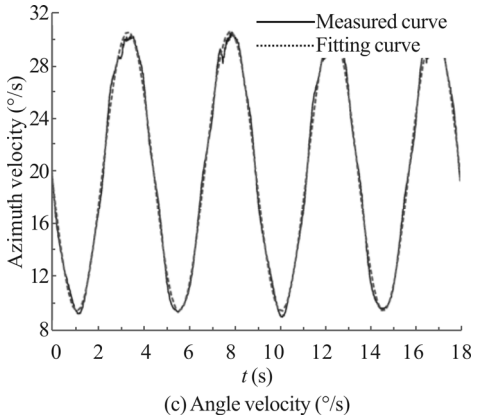

(c) Angle velocity (°/s)

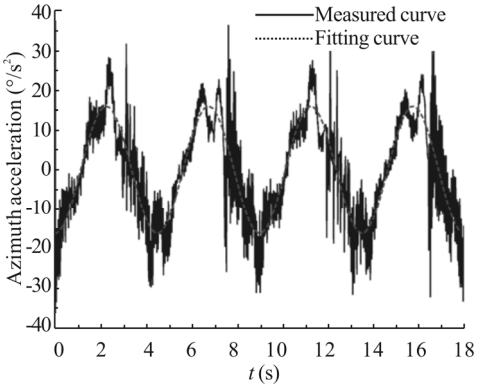

(d) Angle acceleration (°/s²)

Fig.7 The angular motion and the tracking error curves of the azimuth

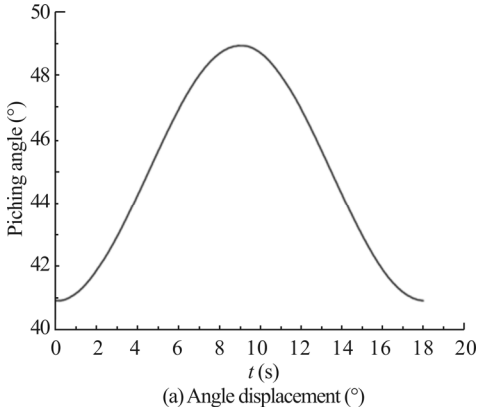

(a) Angle displacement (°)

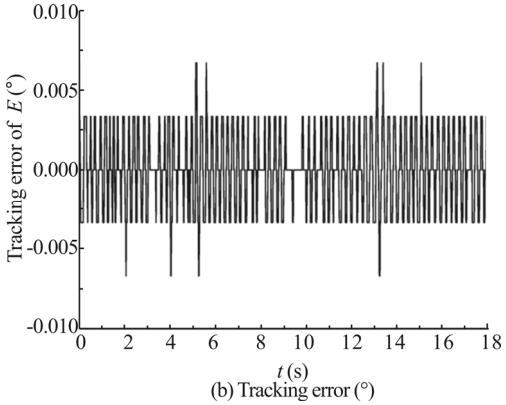

(b) Tracking error (°)

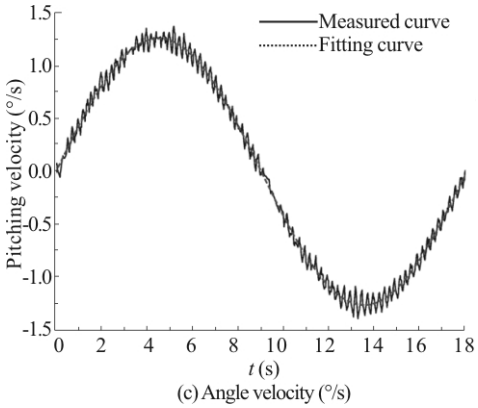

(c) Angle velocity (°/s)

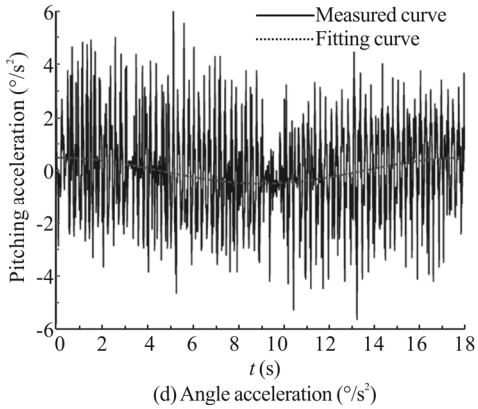

(d) Angle acceleration (°/s²)

Fig.9 The angular motion and the tracking error curves of the pitching

The peak angular motion and the error data of the theodolite can be obtained by theoretical calculation and measured curves as shown in Tab.2. The peak angular velocity error is 2% and the peak angular acceleration error is 14.8%, and the measured tracking error is better than the given theodolite tracking precision index. The range and maneuverability of the pitching motion are small, and the tracking error is superior to that of the azimuth motion. The azimuth motion reflects the maneuverability of the theodolite, and the tracking error measured at this time can be used as the basis for evaluating the tracking performance.

The tracking accuracy of different simulation trajectories is different for the same theodolite tracking

system. The sine angular trajectory used in this paper improves the tracking accuracy under the condition of satisfying the maximum motion maneuverability of theodolite, which shows that the TAT is able to realize the infield physical simulation of the target trajectory, and complete the tracking detection of the photoelectric turntable indoor under the motion maneuverability index.

Tab.2 Comparison of theoretical and measured angular motion peak values and the tracking errors

		Displacement (°)	Peak velocity (°/s)	Peak acceleration (°/s^2)	Tracking error (')
Azimuth	Theoretical value	360	30	14	0.72
	Measured value	359.95	30.62	16.08	
Pitching	Theoretical value	8	1.4	0.49	0.16
	Measured value	8	1.26	0.49	

In summary, the internal physical simulation of the sine angle trajectory at a certain horizontal height is realized by the TAT, which fills the V-Zone of tracking movement with the uniform circumferential characteristics, make the target motion trajectory be designed in the light of the different maneuverability indexes of the photoelectric turntable, and improve the value adaptability of the peak angular acceleration of the target to the peak angular velocity. So the tracking performance test is ensured to be carried out under the maximum maneuvering condition of the photoelectric turntable. The physical simulation of flight trajectory provides feasible conditions for the transformation of the actual target trajectory to the internal field, and provides a practical tracking target for the photoelectric turntable, which is of great engineering application and research value for the accurate evaluation of the tracking accuracy of the photoelectric turntable in the infield environment.

References

[1] Miao Li and Huibin GAO, Research on Computer Control Strategy for Optical Electric Tracking System, International Conference on Mechatronics and Automation, 1670 (2011).

[2] Gabriel Dadalto Mendes Martins, Isutomu de Lima Naruto, Patrícia Danner and Victor Baptista Frencl, A Trajectory Simulator Using Frenet-Serret Formulas Applied to Punctual Objects, 13th IEEE International Conference on Industry Applications, 750 (2018).

[3] Yi Zhu, Xin Chen and Chuntao Li, International Journal of Aerospace Engineering **2016**, 3406256 (2016).

[4] CHEN Kai, WEI Feng, ZHANG Qian-cheng, YU Yun-feng and YAN Jie, Journal of Chinese Inertial Technology **22**, 486 (2014). (in Chinese)

[5] Xiaofei Chang, Tao Yang, Jie Yan and Mingang Wang, Design and Integration of Hardware-in-the-Loop Simulation System for Certain Missile, ICSC, Part II, Communications in Computer and Information Science 327, 229 (2012).

[6] Stephen Steffes, Malak Samaan, Michael Coradt and Stephan Theil, Reconfigurable Hardware-in-the-loop Test Bench for the SHEFEX2 Hybrid Navigation System Experiment, AIAA Modeling and Simulation Technologies Conference, 6331 (2011).

[7] LI Guang-xin, MAO Yu-liang and SONG Chun-lei, Design and Simulation of Trajectory Generator, 4th International Conference on Intelligent Human-Machine Systems and Cybernetics, 201 (2012).

[8] Shuang Cui, Yan Li, Guoquan Yu, JianJun Wang and Ming Lu, The Research and Implementation of the Method of the Photoelectric Theodolite Simulation, International Conference on Advanced Computer Theory and Engineering V6, 382 (2010).

[9] Wang TingTing, Bai Bing, Yuan Yi Fang and Zhu Yong Wei, Research on UAV Simulation Training System Based on Visual Simulation, International Conference on Mechatronics and Automation, 1972 (2018).

[10] Kai Song, Hong Xu, Yan Ding and Hao Li, A Target Tracking Realization Method of UAV Simulation Training System, International Conference on Control, Automation, Robotics & Vision, 1 (2016).

[11] Gu Yingying, Shen Xiangheng and He Gengxian, Opto-Electronic Engineering **38**, 19 (2011). (in Chinese)

[12] Yong-qing Yang, Peng Liu, Wen-ji Shen and Jun-feng Han, Simulation Design of Space Target Tracking System Based on Radial Motion Principle, 4th Seminar on Novel Optoelectronic Detection Technology and Application, 1 (2018).

[13] ZHANG Shao-jun, GAO Yun-guo and XUE Xiang-yao, Optoelectronics Letters **14**, 0461 (2018).

[14] Mariano Lizarraga, Renwick Curry and Gabriel Hugh Elkaim, Flight Test Results for an Improved Line of Sight Guidance Law for UAVs, American Control Conference, 818 (2013).

[15] Abhishek Manjunath, Parwinder Mehrok, Rajnikant Sharma and Ashwini Ratnoo, Application of Virtual Target based Guidance Laws to Path Following of a Quadrotor UAV, International Conference on Unmanned

Aircraft Systems, 252 (2016).

[16] Antonio Vasilijevic, Kristian Jambrosic and Zoran Vukic, Applied Acoustics **129**, 72 (2018).

[17] Qi Chen, Xugang Wang, Jing Yang and Zhongyuan Wang, Aerospace Science and Technology **87**, 448 (2019).

[18] Mustafa Ekinci and Özgür Selimoğlu, Development of a 0.5m Clear Aperture Cassegrain Type Collimator Telescope, Advances in Optical and Mechanical Technologies for Telescopes and Instrumentation II, 991253 (2016).

[19] Yang Juqing, Wang Dayong and Zhou Weihu, Optik **131**, 994 (2017).

[20] ZHANG Ning, SHEN Xiang-heng, YANG Liang and XIE Ming-ming, Optics and Precision Engineering **18**, 1286 (2010). (in Chinese)

[21] Miao Li and Huibin GAO, Advanced Materials Research **472**, 1383 (2012).

[22] Hossein Golnabi, Robotics and Computer Integrated Manufacturing **18**, 187 (2002).